7

Detecting Coronary Layers in IVUS Pictures Using Image Fusion Approach

Ahmad Ashoori, Behzad Moshiri and Seyed Kamaledin Setarehdan
Control and Intelligent Processing Centre of Excellence,
School of ECE, University of Tehran,
Tehran,
Iran

1. Introduction

Coronary artery disease is considered as the most important cause of death in most developed or semi-developed societies. It is known as a silent disease because it develops gradually without any serious symptoms and is recognized only after patient sudden death or serious infarction. The main cause of this type of disease is the plaque integration inside the coronary arteries. This obstructs blood circulation and cardiac muscles nutrition. Hence, finding methods for detecting vessels obstruction and curing it in time would be important to prevent complete obstruction. X-ray Angiography is one of the common methods to this end, which is an invasive method with a high risk due to X-ray radiations. In addition, this method is not strong enough to determine the quantity and the kind of the plaques (Fibrous Tissue, Necrotic Core classification, and/or Fibro-Fatty) (Agostoni et al., 2004).

One of the recent methods emerged for detecting vessels obstruction is Intra Vascular Ultra Sound (IVUS) imaging technique, which is based on inserting an ultrasound catheter inside a vessel and producing real-time cross-sectional images from the inner side of the vessel (Schoenhagen and Stillman, 2005). This semi-invasive method has not the X-ray harms and provides more accurate information from the vessel wall (Schoenhagen and White, 2003). In addition to its safety, IVUS is a reproducible method for imaging the vessel walls and determining the quantity of the vessel obstruction by the plaques. Fig. 1 shows a sample IVUS picture. IVUS imaging is carried out by inserting a catheter into a vessel, which travels through and reaches the artery. Since the area of this catheter is larger than the one of coronary vessels, it stops there and a fine probe (0.96- 1.17 mm long) emerges from it and penetrates to the end of the vessel. The probe is then pulled backward with a constant velocity and meanwhile IVUS frames are captured. Common frequency for imaging is 20-40 MHz. An increase in the frequency may improve the resolution; But due to energy absorption in tissues, quality of the images are low.

For medical usage of IVUS images, the borders of the inside and outside of a vessel and also plaque layers must be determined. This is usually done manually by a specialist, which is a time-consuming and error-prone procedure. Moreover, due to different noises such as motion artifact, ring-down, and speckle noise, automatic processing (Terzopoulos and Fleischer, 1988) of these images is one of the difficult problems in image processing. Lots of

Fig. 1. A sample IVUS picture

efforts have been made to develop an accurate automated method for detection of the regions of interest in IVUS images (Sonka et al., 1995; Zhang et al., 1998; Takagi et al., 2000; Kovalski et al., 2000; Shekhar et al., 1999). Proposed methodologies usually take the advantage of characteristic appearance of arterial anatomy in two-dimensional IVUS images. Several segmentation methods have also been proposed. Some of earlier works on segmentation of IVUS images were based on heuristic graph searching algorithms using a cost function, in which a priori information of the expected pattern in IVUS frames was incorporated (Zhang et al., 1998; Takagi et al., 2000). A class of methods, based on expected similarity of the regions of interest in adjacent IVUS frames, takes into account that the sequence of frames constitutes a three-dimensional object. Under this perspective, active contour principles (Kovalski et al., 2000; Shekhar et al., 1999) could be used to extract the desired lumen and media–adventitia borders.

In this article, the IVUS images of NIOC hospital are to be processed. Section 2 discusses about the deformable models, which are going to be exploited to detect the coronary layers. According to low quality of these images, pre-processing actions including substituting catheter region with the average brightness of the whole image, wavelet transform and edge-preserving smoothing are performed in section 3. Section 4 discusses about detecting the borders applying deformable models (Terzopoulos and Fleischer, 1988), where distance-potential snake is used according to these images topology. The merit of this method comparing with the method presented in (Plissiti et al., 2004), which uses a neural network is its execution time. In section 4, using fuzzy integral operators for fusion in three levels including data-level (before pre-processing), feature-level (after pre-processing) and decision-level (after finding borders in each sample), the process explained in section 4.1 is done again in 4.2 and the results are compared with the previous one. Finally, in section 5, the good effect of image fusion on the IVUS frames of NIOC hospital dataset has been discussed.

2. IVUS image processing methods

Healthy arteries have three layers in IVUS images: 1) the inner layer, Intima; 2) the middle layer, Media; 3) the outer layer, Adventitia. The acoustic impedance difference between cell walls causes these layers to be displayed in these images. These layers' diameters in a healthy person are constant in a vessel from beginning to the end and any change is a symptom of disease.

As mentioned before, finding manually detecting of borders in IVUS images to be time consuming and error prone, lead to introduce automated methods for that. Common edge detection methods such as Sobel mask does not succeed in this task (Paul et al., 1996) (Fig. 2), since these images are perturbed with special noises such as ring down and speckle. Other methods based on first order derivative such as Laplacian or Prewitt mask do not succeed either (Zhu et al., 2002; Gil et al., 2000) (Fig. 3).

Fig. 2. The border detected by the Sobel mask

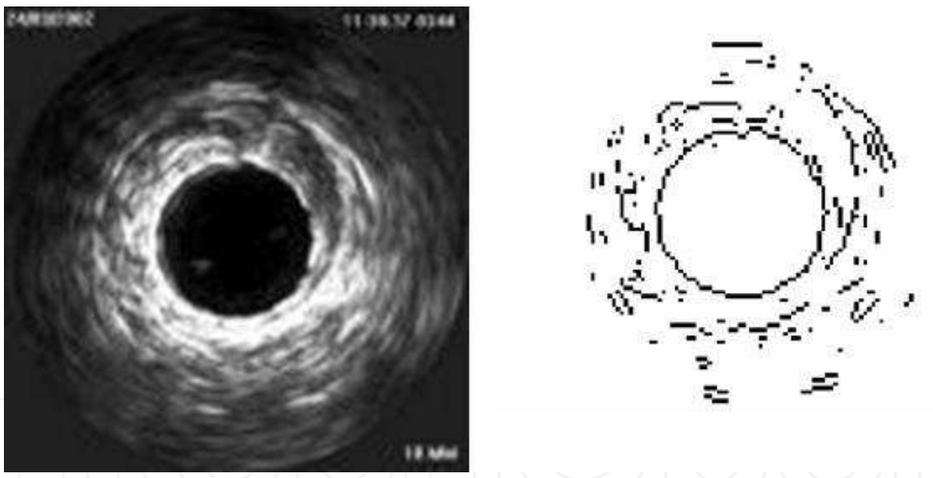

Fig. 3. The border detected by the Prewitt mask

2.1 Deformable models

Introduction of deformable models (active contours) by Kass et al. (Kass et al., 1987) led to extreme progress in edge detection. Active contours move under the influence of internal forces within the curve itself and external forces derived from image data. The internal and external forces are defined so that the active contour will conform to a boundary or other desired features within an image. They are widely used in many applications, including edge detection (Kass et al., 1987), segmentation (Leymarie and Levine, 1993; Durikovic et al., 1995), shape modeling (Terzopoulos and Fleischer, 1988; McInerney and Terzopoulos, 1995), and motion tracking (Terzopoulos and Szeliski, 1992).

There are two main categories of deformable models: parametric (also known as snakes) (Kass et al., 1987) and geometric (Caselles et al., 1993; Malladi et al., 1995). In this paper, we focus on snakes, which synthesize parametric curves within an image domain and allow them to move toward desired features, usually edges. Snakes are usually drawn toward the edges by potential forces, which are defined to be the negative gradient of apotential function. Some extra forces, such as pressure forces (Cohen, 1991), together with the potential forces comprise the external forces. There are also internal forces designed to hold the curve together (elasticity forces) and to keep it from bending too much (bending forces) (Xu and Price, 1997).

2.2 Parametric active contours (Snakes)

A traditional snake is a curve in the form of a rubber object that moves through an image to minimize the following energy function (Xu and Price, 1997):

$$E = \int_0^1 \tfrac{1}{2}[\alpha\left|x'(s)\right|^2 + \beta\left|x''(s)\right|^2] + E_{ext}(x(s))ds \tag{1}$$

In which, α is tension factor in order to control the elasticity energy and β is the rigidity factor in order to control the bending energy and *x(s)* denotes the curve. These two form the internal energy of the snake. The other term in Eq. (1) is external energy, which is obtained from image derivative. Having a gray-level image read in MATLAB software as *I(x,y)*, the common external energy functions can be described:

$$E_{ext}^{(1)}(x,y) = -\left|\nabla I(x,y)\right|^2 \tag{2}$$

$$E_{ext}^{(2)}(x,y) = -\left|\nabla[G_\sigma(x,y) * I(x,y)]\right|^2 \tag{3}$$

In which $G_\sigma(x,y)$ is a two dimensional Gaussian function with the standard deviation σ and ∇ is the gradient operator. Actually, there are more external energy functions that are mostly used for special images, which is not mentioned here. It is obvious from the Eq. (2) and Eq. (3) that the larger the σ is, the more dark the edges will be; but these large standard deviations are needed to increase capture range for the snake (Cohen, 1991; Leroy et al., 1996; Cohen and Cohen, 1993).

The snake, which is going to minimize *E* has to satisfy the Euler equation:

$$\alpha x''(s) - \beta x'''(s) - \nabla E_{ext} = 0 \tag{4}$$

The aforementioned equation can be rewritten as a force equation:

$$F_{\text{int}} + F_{ext}^{(p)} = 0 \tag{5}$$

In which $F_{\text{int}} = \alpha x''(s) - \beta x'''(s)$ and $F_{ext}^{(p)} = -\nabla E_{ext}$. The internal force opposes bending and extra elasticity, while the external force pushes snake to the desired edges. To solve Eq. (4), snake *x* has been considered to be dynamic with respect to time. Now, differentiating with respect to time gives:

$$x_t(s,t) = \alpha x''(s) - \beta x'''(s,t) - \nabla E_{ext} \tag{6}$$

In when the left term reaches zero Eq. (4) will be derived. A numerical solution for Eq. (6) can be found using discretizing the system and solving it iteratively.

2.3 Snakes' problems

There are two main problems dealing with parametric active contours. First, the initial contour must be near the correct border or the algorithm would not work efficiently. In Fig. 4.a an example of converging to a wrong border is provided. Some methods to solve this problem have been proposed including multi-resolution methods (Leroy et al., 1996), pressure forces (Cohen, 1991), distance potentials (Cohen and Cohen, 1993), whose main idea is to increase external forces capture range and drawing the contour to desired edges.

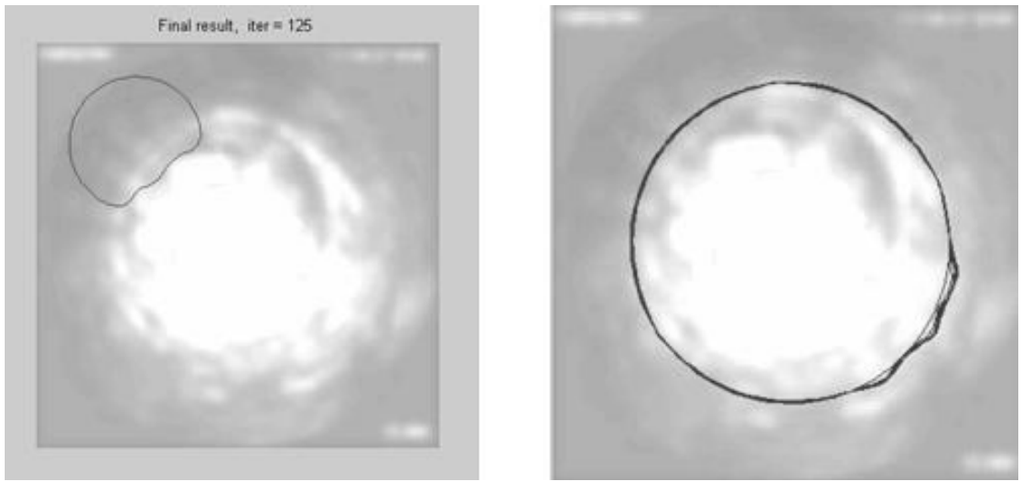

Fig. 4. a) left - Snake has converged to q wrong border. b) right - snake incapability of progressing to very concave edges

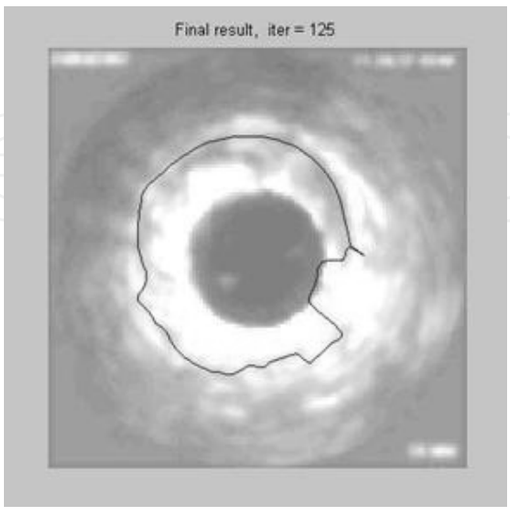

Fig. 5. The border detected by the distance potential snake algorithm applied on a raw image

The second problem is snake incapability of progressing to very concave edges (Davatzikos and Prince, 1995; Abrantes and Marques, 1996). Although some methods such as pressure forces (Cohen, 1991), control points (Davatzikos and Prince, 1995), directional attraction (Abrantes and Marques, 1996), and domain adaptivity (Davatzikos and Prince, 1994) have been emerged, but an acceptable solution has not been developed yet. However, these methods usually solve a problem, while creating another one. For instance, the multi-resolution methods solve the capture range problem, but the snake movement in points with different resolutions goes in trouble. Pressure forces also are very sensitive to the initial contour position. This problem is depicted in Fig. 4.b.
In this work, distance potential snake has been exploited to solve the aforementioned problems and its result is provided in Fig. 5, but still needs to be improved. Hence, before applying the snake (Kass et al., 1987) algorithm (which is active contour based on distance potentials) to the image, some pre-processing actions are performed first. The block diagram of the proposed algorithm for automatic coronary borders extraction is shown in Fig. 6. The blocks would be explained in the following section.

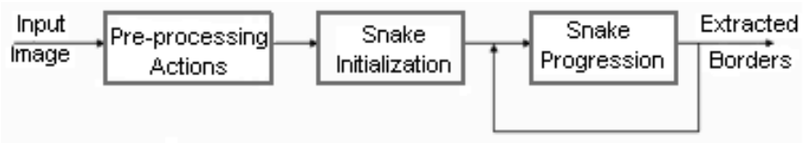

Fig. 6. Detection Algorithm Block Diagram

3. IVUS images pre-processing

Three phases of pre-processing are used in this part, which are a) detection of the catheter region and its substitution by mean value of darkness of the whole image, b) edge-preserving smoothing, and c) wavelet transform.

3.1 Catheter region substitution

The catheter region in the image has edges with very high darkness and is detected as a vessel edge when different deformable models are applied to the image. In this part, this region is detected and substituted with the average darkness of the whole image pixels. It is noticeable that detecting the catheter region is done using a method called region growing, which is going to be fully explained in the next part. This method is based on beginning from one arbitrary pixel of the image comparing the darkness of adjacent pixels to that pixel and this continues until the darkness differs very much. This difference is measured using a suitable threshold. The set of those pixels are considered as a segment, which is the catheter segment in this part.

3.2 Edge preserving smoothing

Most of applications tend to preserve the edges in smoothing procedure. To achieve this goal, some methods have been propounded, which are known as edge-preserving smoothing methods. The most famous algorithms of this family are averaging and median filtering, in which each pixel is substituted with the average or median of its neighbor pixels. Although they cancel the effect of salt and pepper noise very well, but they do not succeed to do so in parts of the image, which are smaller than half of the filter window.

In the method used in this article, the image is firstly segmented and then smoothed. In the smoothing process, the final value of each pixel in the smoothed image is mostly affected by the pixels with similar darkness to it and this makes the result image more useful for edge detection applications. Therefore, inter-region smoothing is avoided and intra-region smoothing is performed instead. Hence, segmentation must be performed first. An algorithm based on region growing (Xiaohan and Yla-Jaaski, 2000) is used for the segmentation. This algorithm is based on beginning from one point, selecting a suitable threshold, and comparing the neighbor pixels darkness with this threshold, which leads to the fact that whether this pixel is in that region or not. An algorithm for implementing the region growing is presented in (Xuan et al., 1995). Nevertheless, in different region growing algorithms a pixel is usually appended to a region if its darkness intensity is within a certain level from that region. This condition has not proven to be efficient in noisy images. Hence, this condition has been substituted with two other conditions here: a) in addition to comparing pixel intensity with the center pixel of a region, its intensity is also compared with that of the pixel neighbor to the center pixel as well. Assuming the independency of the noise in each pixel, if the probability of appending a wrong pixel to a region was p in common algorithms, it would reduce to p^2 here. Although this condition improves the known region algorithm performance, but it is a bit conservative and it makes the possibility of not appending a right point to a region more. So, another condition must also be taken into account: b) if the center pixel similarity to its neighbor pixel in one direction (i.e. up, down, left, or right) was more than its similarity to its neighbor of neighbor pixel in the same direction, then the neighbor pixel belongs to the center pixel region. Similarity of two pixels is defined as absolute value of their intensity difference.

After detecting a region, a pixel outside this region is chosen and this process is repeated until the whole image is segmented. When the segmentation is finished, a Gaussian filter is applied to (convolved with) each region according to its darkness.

3.3 Wavelet transform

Image analysis and processing using wavelet transform is one of the recent approaches in signal and image processing. Image processing using wavelet transform usually includes applying two-dimensional wavelet transform to the image, making suitable changes in the wavelet domain, and using inverse wavelet transform. In the third phase of the pre-processing part, wavelet transform is applied to the image in one level, which results the resolution decreased to half and hence, detecting the edges would be easier. The whole three phases done on a sample image is shown in Fig. 7.

4. Detecting coronary layers using deformable models

4.1 Detecting coronary layers in a single pre-processed IVUS picture

Once the image went through the pre-processing phase, it is ready to be used for applying deformable models to find the coronary layers. Here, detecting the internal layer i.e. intima-media has been focused; Nevertheless, the same algorithm could be applied to find the media-adventitia border as well. The snake initialization would be slightly different in that case.

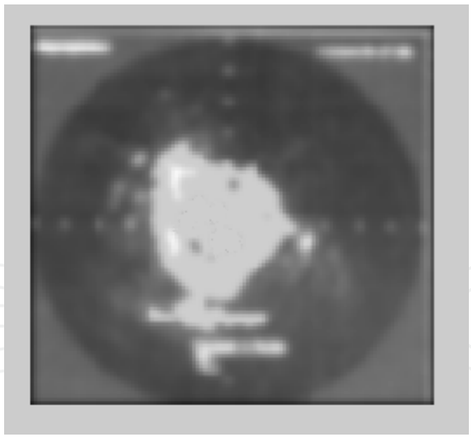

Fig. 7. Edge preserved smoothed picture of an IVUS image, in which the catheter region is substituted after applying one level wavelet transform.

Distance potential snake has been utilized according to the topology of this kind of images to find the borders. Somewhere a bit outsider of the detected catheter region has been considered as the initial state of the snake in order to overcome the drawbacks mentioned in section 2.3. This is an important advantage, which makes this method completely automatic while similar approaches need the initial contour to be made manually (Plissiti et al., 2004). The algorithm was implemented in MATLAB and the results on the pre-processed image (Fig. 7) are provided in Fig. 8.

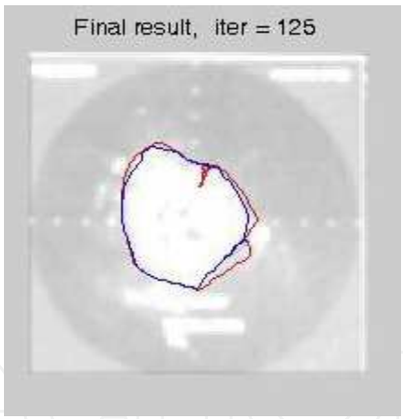

Fig. 8. Detected region as the internal border in one pre-processed image – Red border is detected by the algorithm and blue border is detected by a specialist

As can be seen in the picture, due to existence of ring-down noise in some parts of the image, the snake has moved neither to the inside nor to the outside in those regions.
It is also interesting that the sharp point observed in the picture is due to the speckle noise, which has affected the image in that area. The efficiency of this algorithm in detecting the true border on a single image is 88.42%.

4.2 Detecting coronary layers in fused IVUS pictures

Information fusion is used in many applications nowadays. In this paper, fusion of the images' information (Singh et al., 1996) with fuzzy approach is taken into action. Image

fusion is used in several industrial and medical applications in order to get a more efficient image. Image fusion has the following advantages: a) Taking into account extra information (redundancy), increases the reliability; b) It improves the image capabilities as it keeps complementary information (Fig. 9).

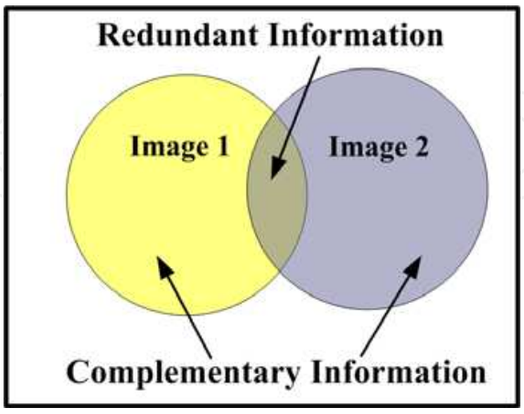

Fig. 9. Image fusion characteristics

Fuzzy approach to this context is very useful, when there is uncertainty and no mathematical relations. Each IVUS frame in a sequence of frames obtained from the same arterial segment can be considered quite similar to the previous one. In this paper, fusion of some IVUS sequential frames, having energy difference less than 10% of each, is exploited using fuzzy integral operators.

4.2.1 Fuzzy integral operators

Two great categories for fuzzy information fusion exist, which are Choquet and Sugeno fuzzy integral operators (Yager, 2004). These operators are based on the fuzzy measured data. It is translated as the gray-scale of any pixel in the image, which is a number between zero and one. The Choquet discrete fuzzy integral operator based on the mentioned fuzzy measures $a_1,...,a_n$, which belong to $[0,1]$ is described as:

$$C_\mu(a_1,a_2,...,a_n)=\sum_{i=1}^{n}(a_{(i)}-a_{(i-1)})\mu(A_{(i)}) \tag{7}$$

And the Sugeno discrete fuzzy integral operator based on the fuzzy measures $a_1,\ldots,a_n$, which belong to *[0,1]* is described as:
in which $a_{(0)}=0$ and $i=1,2,\ldots,n$ is a permutation of a_i s such that $a_{(1)}\le a_{(2)}\le\ldots\le a_{(n)}$ and $A_{(i)}=\left\{x_{(1)},x_{(2)},\ldots,x_{(n)}\right\}$.

$$S_\mu(a_1,a_2,...,a_n)=\underset{i=1}{\overset{n}{Max}}(Min(a_{(i)},\mu(A_{(i)}))) \tag{8}$$

in which $a_{(0)}=0$ and $i=1,2,\ldots,n$ is a permutation of a_i s such that $a_{(1)}\le a_{(2)}\le\ldots\le a_{(n)}$ and $A_{(i)}=\left\{x_{(1)},x_{(2)},\ldots,x_{(n)}\right\}$.

The Choquet integral is stable under positive linear transformations, while the Sugeno integral is stable under similar transformations with minimum and maximum replaced by product and sum respectively. This property makes the Sugeno integral more suitable for ordinal aggregation (where only the order of the elements is important) while the Choquet integral is suitable for cardinal aggregation (where the distance between the numbers has a meaning).
The generalized characteristics of these two integrals are remarkable. The Choquet integral is the generalized form of the ordered weighted average (OWA) operator, while the Sugeno integral generalizes the weighted minimum and the weighted maximum. The corresponding parameters to create a certain operator with these operators are shown in Tables 1, 2.

	Choquet Integral
Minimum	$\begin{cases}\mu(A)=1 & if\ A=C\\ \mu(A)=0 & otherwise\end{cases}$
Maximum	$\begin{cases}\mu(A)=0 & if\ A=\varphi\\ \mu(A)=1 & otherwise\end{cases}$
k-order statistics	$\begin{cases}\mu(A)=0 & if\ card(A)\le n-k\\ \mu(A)=1 & otherwise\end{cases}$
Arithmetic mean	$\mu(A)=\frac{card(A)}{card(C)}$
Weighted mean	$\mu(A)=\sum_{x_i\in A}\left[\mu\{x_i\}\right]$ $and\ \ \mu\{x_i\}=w_i\ \ for\ all\ i$
OWA	$\mu(A)=\sum_{j=0}^{card(A)-1} w_{n-j}$

Table 1. Choquet integral special cases

	Sugeno Integral
Minimum	$\begin{cases}\mu(A)=1 & if\ A=C\\ \mu(A)=0 & otherwise\end{cases}$
Maximum	$\begin{cases}\mu(A)=0 & if\ A=\varphi\\ \mu(A)=1 & otherwise\end{cases}$
k-order statistics	$\begin{cases}\mu(A)=0 & if\ card(A)\le n-k\\ \mu(A)=1 & otherwise\end{cases}$
Weighted minimum	$\mu(A)=1-\max_{x_i\in A}\left[\mu\{x_i\}\right]$ $and\ \ \mu\{x_i\}=w_i\ \ for\ all\ i$
Weighted maximum	$\mu(A)=\max_{x_i\in A}\left[\mu\{x_i\}\right]$ $and\ \ \mu\{x_i\}=w_i\ \ for\ all\ i$

Table 2. Sugeno integral special cases

The only problem using these integrals is the number of 2^n weights to be determined, for a simple n criteria aggregation. These weights are nothing, but the characterization of fuzzy measures. Some solutions have been proposed to reduce the number of these weights: An interesting approach was proposed by Grabisch in (Grabisch, 1996), in which he suggests to use k-additive fuzzy measures. The idea is to define measures that are multilinear of degree k, i.e. if $card(A) > k$ then $\mu(A) = 0$. This approach allows the model the strength of small coalitions and reduces the number of weights to $\sum_{i=1}^{k} C_n^i$ instead of 2^n.

Another approach, which is used here is to determine the weights by training on examples, in which at least $\frac{n!}{[(n/2)!]^2}$ training vector is needed.

However, the Choquet and Sugeno fuzzy integral operators have fundamental difference; Because the former is based on linear operators, while the latter is based on nonlinear *Max* and *Min* operators. The relationships between different aggregations and fuzzy integral operators are provided in Fig. 10.

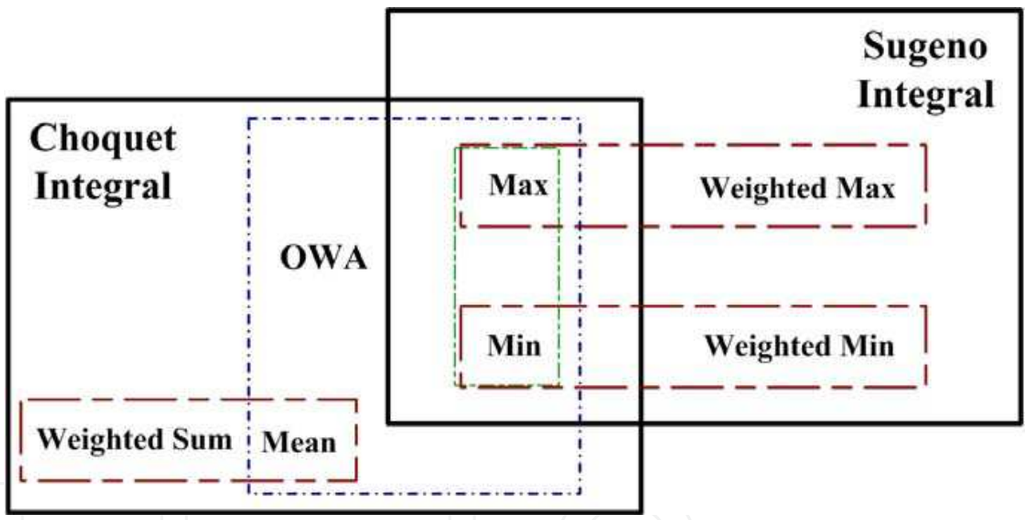

Fig. 10. The relationships between different aggregations and fuzzy integral operators

4.2.2 Applying the algorithm on fused frames

Information fusion can be performed in different levels. If this fusion is to be performed on data level, the samples of IVUS frames must be fused initially, then the pre-processing actions has to be performed and finally detecting the borders applying deformable models would be executed. If the fusion is to be performed on feature level, the pre-processing actions ought to be performed on each frame initially, the obtained images would be fused next, and the algorithm for detecting the borders would be executed finally. And if the fusion is intended to be performed on decision level, the pre-processing actions are to be performed on each frame initially; the borders are to be detected applying the algorithm to each frame next, and the result borders fused eventually. The images information fusion block diagram is provided in Fig. 11.

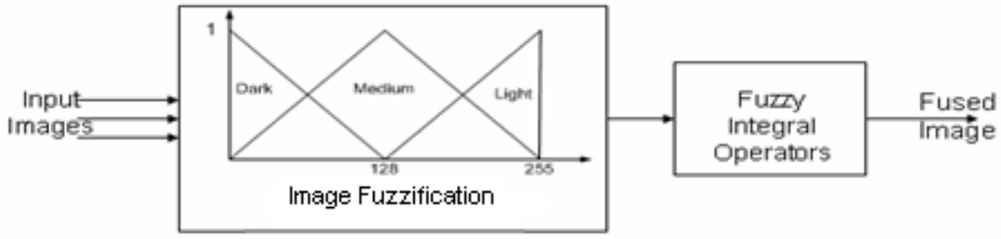

Fig. 11. Fuzzy image fusion block diagram

The results of the algorithm explained in the section 3 on fused frames would be studied in the following. Fig. 12 shows the border detected by the snake algorithm applied on the fused image using Sugeno operator in data level compared with the one detected by the specialist.

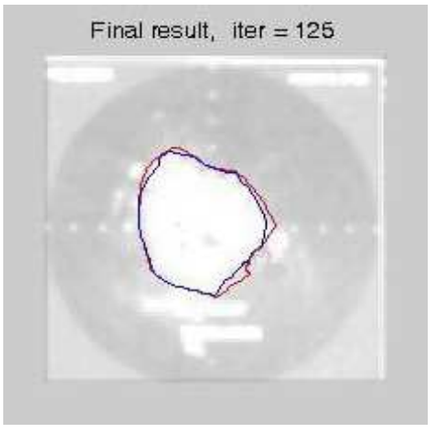

Fig. 12. The border detected by the snake algorithm applied on the fused image using Sugeno operator in data level– Red border is detected by the algorithm and blue one is detected by the specialist

The border detected by the snake algorithm applied on the fused image using Sugeno operator in feature and decision level compared with ones detected by the specialist are provided in the figures 13, 14 respectively.

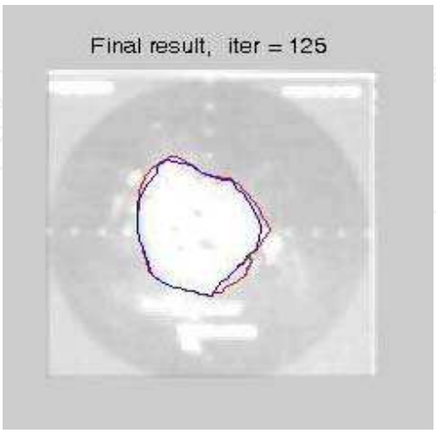

Fig. 13. The border detected by the snake algorithm applied on the fused image using Sugeno operator in feature level– Red border is detected by the algorithm and blue one is detected by the specialist

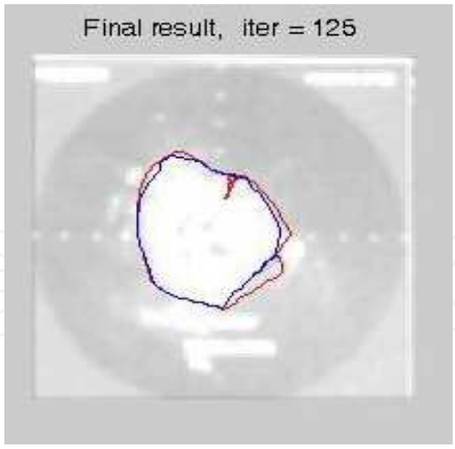

Fig. 14. The border detected by the snake algorithm applied on the fused image using Sugeno operator in decision level– Red border is detected by the algorithm and blue one is detected by the specialist

The higher level the fusion is performed, the more is affected the result by noise. This is due to the special noises of the images of this type (IVUS), which deviates the snake from the correct border and if an error occurs, its correction in higher levels is almost irreparable.
Quantitative comparisons between fuzzy integral operators used in different levels of fusion, are shown in Table 3. The numbers in the table are the algorithm efficiency in finding the borders detected by the specialist.

	Fusion using Choquet fuzzy integral operator	Fusion using Sugeno fuzzy integral operator
Data Level Fusion	91.87%	93.125%
Feature Level Fusion	90.42%	91.58%
Decision Level Fusion	88.96%	89.11%

Table 3. Quantitative comparison between fuzzy integral operators used for fusion in different levels

5. Conclusion

In this article, taking into account the low quality of the IVUS images, edge-preserving smoothing and also wavelet transform were performed as pre-processing actions in order to improve the performance of detecting the coronary layers. Detecting the borders using deformable models was performed next; but due to the especial imaging noises of the IVUS pictures, fusion of these images verified efficient. Using fuzzy integral operators in three levels

including data, feature and decision the images were fused, in which detecting borders in the fused images using Sugeno operator, and in data level was more successful than the others. This method has the advantage of being fully automated, without needing the initial contour to be manually assigned. The merit of this method comparing with similar methods is also its acceptable executing time, which is very important for curing patients.

6. Acknowledgment

The authors would like to thank the NIOC hospital for its support from this project. They especially thank Dr.Ghaziani because of her infinite endeavor for providing the dataset for this work.

7. References

Abrantes, A. J. & Marques, J. S. (1996). *A class of constrained clustering algorithms for object boundary extraction*, IEEE Trans. Image Processing, vol. 5, pp. 1507–1521

Agostoni, P.; Schaar, J. A. & Serruys, P. W. (2004). *The challenge of vulnerable plaque detection in the cardiac catheterization laboratory*, Kardiovaskuläre Medizin

Caselles, V.; Catte, F.; Coll, T. & Dibos, F. (1993). *A geometric model for active contours*, Numerische Mathematik, 66, 1–31

Cohen, L. D. (1991). *On active contour models and balloons*, CVGIP: Image Understanding, 53(2): 211–218

Cohen, L. D. & Cohen, I. (1993). *Finite-element methods for active contour models and balloons for 2-D and 3-D images*, IEEE Trans. Pattern Anal. Machine Intell., vol. 15, pp. 1131–1147

Davatzikos, C. & Prince, J. L. (1994). *Convexity analysis of active contour models*, in Proc. Conf. Information Science and Systems, pp. 581–587

Davatzikos, C. & Prince, J. L. (1995). *An active contour model for mapping the cortex*, IEEE Trans. Med. Imag., vol. 14, pp. 65–80

Durikovic, R.; Kaneda, K. & Yamashita, H. (1995). *Dynamic contour: A texture approach and contour operations*, Vis. Comput., vol. 11, pp. 277–289

Gil, D.; Radeva, P. & Saludes, J. (2000). *Segmentation of artery wall in coronary IVUS images: A Probabilistic Approach*, ICPR, pp.4352, 15th International Conference on Pattern Recognition (ICPR'00) - Volume 4

Grabisch, M. (1996). *k-additive fuzzy measures*, 6th International Conference on Information Processing and Management of Uncertainty in Knowledge-Based Systems (IPMU), Granada, Spain, July 1996

Kass, M.; Witkin, A. & Terzopoulos, D. (1987). *Snakes: Active contour models*. Int. J. Computer Vision, 1(4), pp. 321–331

Kovalski, G.; Beyar, R.; Shofti, R. & Azhari, H. (2000). *Three-dimensional automatic quantitative analysis of intravascular ultrasound images*, Ultrasound Med. Biol., vol. 26, No. 4, pp. 527-537

Leroy, B.; Herlin, I. & Cohen, L. D. (1996). *Multi-resolution algorithms for active contour models*, in 12th Int. Conf. Analysis and Optimization of Systems, pp. 58–65

Leymarie, F. & Levine, M. D. (1993). *Tracking deformable objects in the plane using an active contour model*, IEEE Trans. On Pattern Anal. Machine Intell., 15(6): 617–634

Malladi, R.; Sethian, J. A. & Vemuri, B. C. (1995). *Shape modeling with front propagation: A level set approach*, IEEE Trans. on Pattern Anal. Machine Intell., 17(2): 158–175

McInerney, T. & Terzopoulos, D. (1995). *A dynamic finite element surface model for segmentation and tracking in multidimensional medical images with application to cardiac 4D image analysis*, Comput. Med. Imag. Graph., vol. 19, pp. 69–83

Paul, J.; Brathwaite, A.; Chandran, K. B.; McPherson, D. D. & Dove, E. L. (1996). *Lumen Detection in Human IVUS Images using Region-Growing*, IEEE Computer in Cardiology

Plissiti, M. E.; Fotiadis, D. I.; Michalis, L. K. & Bozios, G. E. (2004). *An automated method for lumen and media-adventitia border detection in a sequence of IVUS frames*, IEEE Trans. On Information Tech. in Biomedicine, vol. 8, No. 2

Schoenhagen, J. P. & Stillman, A. E. MD, PhD (2005). *CT of the heart Principles, advances, clinical uses*, Cleveland Clinic Journal of Medicine Vol. 72, No. 2

Schoenhagen, P. & White, R. D. (2003). *Coronary imaging: Angiography shows the stenosis, but IVUS, CT, and MRI show the plaque*, Cleveland Clinic Journal of Medicine Vol. 70, No. 8

Terzopoulos, D. & Fleischer, K. (1988). *Deformable models*, Vis. Comput., vol. 4, pp. 306–331

Shekhar, R.; Cothren, R. M.; Vince, D. G.; Chandra, S.; Thomas, J. D. & Cornhill, J. F. (1999) *Three-dimensional segmentation of luminal and adventitial borders in serial intravascular ultrasound images*, Comput. Med. Imaging Graph, vol. 23, pp. 299-309

Singh, H.; Raj, J.; Kaur, G. & Meitzler, T. (2004). *Image Fusion Using Fuzzy Logic and Applications*, IEEE Trans. Image Processing, vol. 24, pp. 25–29

Sonka, M.; Zhang, X.; Siebes, M.; Bissing, M. S.; DeJong, S. C.; Collins, S. M. S. & McKay C. R. (1995). *Segmentation of Intravasular ultrasound images: A knowledge-based approach*, IEEE Trans. Med Imag., vol. 14, pp. 719-732

Takagi, A.; Hibi, K.; Zhang, X.; Teo, T. J.; Bonneau, H. N.; Yock, P. G. & Fitzgerald, P. J. (2000). *Automated contour detection for high-frequency intravascular ultrasound imaging: A technique with blood noise reduction for edge enhancement*, Ultrasound Med. Biol., vol. 26, No. 6, pp. 1033-1041

Terzopoulos, D. & Szeliski, R. (1992). *Tracking with Kalman snakes*, In A. Blake and A. Yuille, editors, Active Vision, Artificial Intelligence, pages 3–20. The MIT Press, Cambridge, Massachusetts

Xiaohan, Y. & Yla-Jaaski, J. (2000). *A new algorithm for image segmentation based on region growing and edge detection*, IEEE CH 336-4/91/2000

Xu, C. & Prince, L. (1997). *Gradient Vector Flow: A New External Force for Snakes*, IEEE Proc. Conf. on Comp. Vis. Patt. Recog. (CVPR'97), pp. 66-71

Xuan, J.; Adali, T. & Wang, Y. (1995). *Segmentation of magnetic resonance brain image: Integration region growing and edge detection*, in Proc. International Conference on Image Processing (ICIP'95), pp. 544-547

Yager, R. (2004). *Uncertainty Modeling and Decision Support*, Reliability Engineering and System Safety, pp. 341-354

Zhang, X.; McKay, C. R. & Sonka, M. (1998). *Tissue characterization in intravascular ultrasound images*, IEEE Trans. Med. Imag., vol. 17, pp. 889-898

Zhu, H.; Liang, Y. & Friedman, M. H. (2002). *IVUS image segmentation based on contrast*, Proc. SPIE 4684, 1727, DOI:10.1117/12.467143

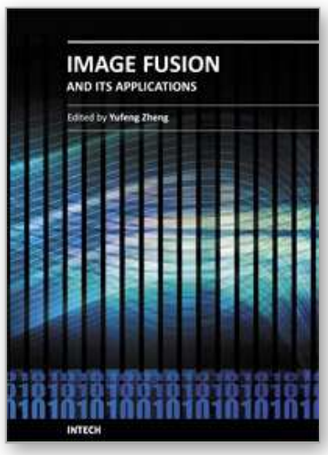

Image Fusion and Its Applications

Edited by Dr. Yufeng Zheng

ISBN 978-953-307-182-4
Hard cover, 242 pages
Publisher InTech
Published online 24, June, 2011
Published in print edition June, 2011

The purpose of this book is to provide an overview of basic image fusion techniques and serve as an introduction to image fusion applications in variant fields. It is anticipated that it will be useful for research scientists to capture recent developments and to spark new ideas within the image fusion domain. With an emphasis on both the basic and advanced applications of image fusion, this 12-chapter book covers a number of unique concepts that have been graphically represented throughout to enhance readability, such as the wavelet-based image fusion introduced in chapter 2 and the 3D fusion that is proposed in Chapter 5. The remainder of the book focuses on the area application-orientated image fusions, which cover the areas of medical applications, remote sensing and GIS, material analysis, face detection, and plant water stress analysis.

INTECH
open science | open minds

InTech Europe
University Campus STeP Ri
Slavka Krautzeka 83/A
51000 Rijeka, Croatia
Phone: +385 (51) 770 447
Fax: +385 (51) 686 166
www.intechopen.com

InTech China
Unit 405, Office Block, Hotel Equatorial Shanghai
No.65, Yan An Road (West), Shanghai, 200040, China
中国上海市延安西路65号上海国际贵都大饭店办公楼405单元
Phone: +86-21-62489820
Fax: +86-21-62489821

IntechOpen